Stable line defects in silicene

Dibyajyoti Ghosh,[1] Prakash Parida,[2] and Swapan K. Pati[3,*]
[1]*Chemistry and Physics of Materials Unit, JNCASR, Bangalore 560064, Karnataka, India*
[2]*Institute for Theoretical Physics, University of Regensburg, D-93040 Regensburg, Germany*
[3]*Theoretical Sciences Unit, JNCASR, Bangalore 560064, Karnataka, India*
(Received 7 July 2015; revised manuscript received 15 October 2015; published 19 November 2015)

Line defects in two-dimensional (2D) materials greatly modulate various properties of their pristine form. Using *ab initio* molecular dynamics (AIMD) simulations, we investigate the structural reconstructions of different kinds of grain boundaries in the silicene sheets. It is evident that depending upon the presence of silicon adatoms and edge shape of grain boundaries (i.e., armchair or zigzag), stable extended line defects (ELDs) can be introduced in a controlled way. Further studies show the stability of these line-defects in silicene, grown on Ag(111) surface at room-temperature. Importantly, unlike most of the 2D sheet materials such as graphene and hexagonal boron nitride, 5-5-8 line defects modify the nonmagnetic semimetallic pristine silicene sheet to spin-polarized metal. As ferromagnetically ordered magnetic moments remain strongly localized at the line defect, a one-dimensional spin channel gets created in silicene. Interestingly, these spin channels are quite stable because, unlike the edge of nanoribbons, structural reconstruction or contamination cannot destroy the ordering of magnetic moments here. Zigzag silicene nanoribbons with a 5-5-8 line defect also exhibit various interesting electronic and magnetic properties depending upon their width as well as the nature of the magnetic coupling between edge and defect spin states. Upon incorporation of other ELDs, such as 4-4-4 and 4-8 defects, 2D sheets and nanoribbons of silicene show a nonmagnetic metallic or semiconducting ground state. Highlighting the controlled formation of ELDs and consequent emergence of technologically important properties in silicene, we propose new routes to realize silicene-based nanoelectronic and spintronic devices.

DOI: 10.1103/PhysRevB.92.195136 PACS number(s): 73.22.−f, 71.15.Mb, 71.15.Pd, 71.55.Ht

I. INTRODUCTION

Successful synthesis and extraordinary properties of graphene, a two-dimensional (2D) hexagonal planar sheet of carbon, have revolutionized low-dimensional material science research [1,2]. Inspired by this, several research groups demonstrated other 2D sheet materials which show promising characteristics, sometimes even better than graphene [3,4]. Among them, silicene, a slightly buckled, hexagonal monolayer sheet of silicon, has already shown a huge possibility to be used in future nanoelectronic devices due to its compatibility with existing silicon-based devices [5–7].

Confirming the earlier theoretical prediction about the existence of silicene [8–10], it has been synthesized successfully on the surface of various substrates such as Ag(111), Ir(111), ZrB_2(0001), etc. [11–14]. Investigations show that like graphene, a free-standing sheet of silicene is a massless, Dirac-fermion-containing, zero-gap semimetal and also possesses high Fermi velocity [9–12,15]. Moreover, due to the buckling nature, silicene becomes superior than graphene in many aspects, such as the enhanced quantum Hall effect, the possibility of band-gap tuning by the perpendicular electric field, better surface reactivity, etc. [6,10,16–18]. Most importantly, in a recent experiment Tao *et al.* successfully fabricated a silicene field-effect transistor and found quite appreciable room-temperature mobility of $\approx$100 $cm^2\ V^{-1}\ s^{-1}$ [19]. This evidently proves silicene as a potential 2D material for next-generation electronic devices.

During the synthesis of any 2D sheet, different kinds of imperfections, such as point defects, vacancies, and adatom adsorption, arise inevitably [20,21]. As demonstrated by several groups, these defects greatly alter the mechanical, electronic, magnetic, and transport properties of pure sheets [22–24]. Interestingly, in the case of silicene, as Si atoms nucleate at a much faster rate due to their low-diffusion barrier on substrates, these defects form more frequently [25–28]. Moreover, these defects modulate some of the above-mentioned properties of a pristine silicene sheet more drastically than those of well-studied graphene [28]. Nonetheless, these defective 2D sheets suffer from poor stability as local structural rearrangements by annealing or chemical passivation can remove the defects easily [29,30]. Importantly, another kind of structurally robust defect is topological line defects, which remain quite stable against local geometrical rearrangements [31–34]. Different types of line defects are already found at the grain boundaries (GBs) of graphene, hexagonal boron nitride, molybdenum disulphide, etc., where they induce significant modification of several properties of these sheets [35–42]. However, creation of topological line defects in a controlled manner is still a challenging task. Several experimental and theoretical reports show that controlled engineering of the GBs during or after synthesis in these 2D materials eventually leads to insertion of different kinds of line defects [31–33,39–41,43]. Interestingly, during the growth of silicene on Ag(111) using the molecular-beam-epitaxy technique, Chiappe *et al.* observed several kinds of GBs [25]. This opens up a huge possibility to modify these GBs in a controlled manner to insert different kinds of line defects.

In the present study, we propose easily achievable ways to insert several kinds of line defects in the free-standing silicene 2D sheet as well as in its nanoribbons by performing constant-temperature *ab initio* molecular dynamics (AIMD)

*pati@jncasr.ac.in

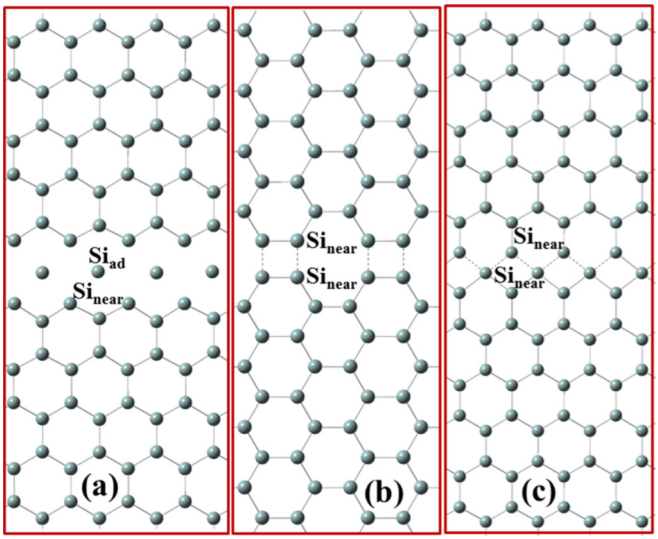

FIG. 1. (Color online) Initial structures (i.e., before reconstruction) of grain boundaries of (a) ZSi-ZSi, (b) ASi-ASi, and (c) ZSi-KSi.

simulations. We also explore the stability of these defective sheets on the surface of Ag(111). Unreactive Ag(111) is the most widely used substrate to synthesize silicene due to its sixfold symmetry and low tendency to form Si-Ag alloy [11]. Further, to investigate the effects of these line defects on electronic and magnetic properties of free-standing silicene and its nanoribbons, we perform density functional theory (DFT) calculations. Note that, because various groups propose different ways, such as insertion of buffer layers [6,44] and utilization of quantum well states of ultrathin metallic substrates [45], to suppress silicene-substrate interactions, we exclude the surface effects during the electronic structure calculations in the present study. It appears that, depending upon the nature of GBs and adatoms, different kinds of line defects, such as a one-dimensional chain of tetragons (4-4-4) or two pentagons and one octagon (5-5-8) or one tetragon and one octagon (4-8), can be embedded in this material. Interestingly, these line defects largely tune the electronic and magnetic behaviors of the silicene sheet and nanoribbons.

In Fig. 1, we present three kinds of initial GBs which can arise during the growth of silicene on the substrate. Importantly, to make our present study more specific and compact, we consider that two crystalline grains meet at the GB face to face, i.e., without forming any misoriented angle there. These structures have already been considered as the initial geometry in other 2D sheet materials to perform *ab initio* molecular dynamics simulations to investigate the formation of line defects [39–41,43]. In the present study, these structures are divided into two types: (1) In Figs. 1(a) and 1(c), two grains of silicene grow adjacent to one another, and their zigzag edges meet at the GB. (2) In Fig. 1(b), armchair edges of grains face each other at the GB. To nomenclature the defects in detail, in Fig. 1(a), two pure zigzag edges construct the GB without any mutual translation followed by the deposition of silicon adatoms at the GB. This system is named ZSi-ZSi. In Fig. 1(c), one zigzag and another Klein edge form the GB without any additional adatoms, and we denote it as ZSi-KSi. Figure 1(b) shows the GB where two pure armchair edges come closer without any adatoms at the GB, and this is named ASi-ASi. During reconstruction, we keep the two nearest extended line defects (ELDs) separated by eight zigzag/armchair chains of Si atoms. Systems with larger ELD separation are also considered to check the impact of defect-defect interaction upon the reconstruction. Moreover, to inhibit the coupling between two ELDs during the calculation of electronic and magnetic properties, we increase the interdefect separation to 18 zigzag/armchair chains. To make the discussion very understandable, the Si atoms deposited at the GB (for ZSi-ZSi) and the Si atoms closest to the GB are labeled Si_{ad} and Si_{near}, respectively [See Fig. 1(a)]. The nanoribbon of these sheets is represented as N-M-XNR, where N and M denote the number of zigzag/dimer lines on the two sides of the ELD and X is the corresponding sheet. The edge atoms of these nanoribbons are labeled Si_{edge}.

II. COMPUTATIONAL DETAILS

We perform constant-temperature AIMD simulations considering the canonical ensemble (NVT) as implemented in the Vienna Ab initio Simulation Package (VASP) [46]. The Perdew-Burke-Ernzerhof (PBE) functional within the generalized gradient approximation (GGA) is used as the exchange-correlation functional [47]. The projected augmented-wave (PAW) potential with a plane-wave basis set having a cutoff of 400 eV is used for all AIMD calculations [48,49]. We use a Nose-Hoover thermostat to adjust the temperature during the simulations, and a time step of 1 fs is considered to integrate the equation of motion [50,51]. To avoid the spurious interaction in the nonperiodic direction we consider a cell of $a \times b \times 15$ Å, where a and b are lattice constant in periodic directions. For 5-5-XNRs and 10-10-XNRs, cells are considered to be $a \times 60 \times 15$ Å and $a \times 120 \times 15$ Å, respectively. To investigate the stability of these reconstructed sheets on the Ag substrate, we consider a rectangular slab of Ag(111) [(3×7) cell of a rectangular unit cell of six Ag atoms], containing three atomic layers. The periodic images are separated from the slab by a vacuum region of 40 Å. The geometry of the Ag slab is relaxed until the forces acting on the atoms become smaller than 0.02 eV/Å. During AIMD computation, to reduce computational cost, we freeze the positions of all Ag atoms, keeping only Si atoms free to move. van der Waals dispersion forces acting between the surface and silicene are incorporated by Grimme's method [52]. To investigate electronic and magnetic properties of these equilibrated, reconstructed, free-standing systems, we carry out DFT-based calculations using VASP. For these calculations, the plane-wave cutoff is considered to be 500 eV, and the k-point mesh for 2D sheets is $9 \times 7 \times 1$ (23 irreducible k points). Test calculations with a higher plane-wave cutoff and denser k mesh show good convergence of the total energy of the systems within the considered values of these parameters. The energy threshold is chosen to be 10^{-8} eV for all static calculations. For nanoribbons, the one-dimensional Brillouin zone is sampled by $31 \times 1 \times 1$ automatic-mesh k points. As pristine and other modified silicene sheets possess a very strong spin-orbit coupling (SOC) effect, we calculate the electronic property of the present systems by incorporating the SOC effect as implemented in the VASP package.

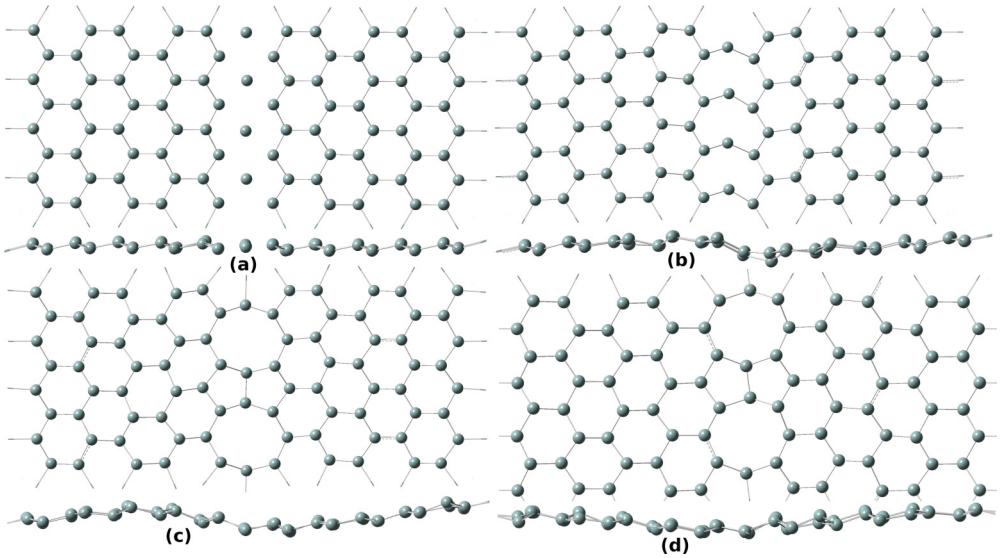

FIG. 2. (Color online) Snapshot of top and side views of ZSi-ZSi during AIMD simulations at constant temperature (300 K) and constant pressure (1 atm) after (a) 0, (b) 0.25, (c) 0.8, and (d) 5 ps.

III. RESULTS AND DISCUSSION

A. Reconstruction in 2D sheets

First, performing the AIMD simulation at 300 K and analyzing the resulting trajectory, we investigate the reconstruction process of the GB for the ZSi-ZSi sheet. As shown in Fig. 2, initially, quite mobile Si_{ad} atoms form bonds with Si_{near} and create a distorted unstable 8-8-8 ELD at the GB [Fig. 2(b)]. However, in the process of equilibration, this unstable ELD gets transformed to a 5-5-8 ELD, where Si_{ad} atoms form a dimer among themselves along with stable covalent bonds with Si_{near} atoms [Figs. 2(c) and 2(d)]. The variation of potential energy of the system with simulation time, shown in Fig. 3, evidently indicates that formation of a 5-5-8 ELD stabilizes the reconstructed sheet. Fundamentally, strong covalent bond formation among the initially nonbonded Si_{ad} atoms causes this structural stabilization. Although the potential energy of the sheet shows little oscillating behavior, we do not observe any kind of further reconstruction or out-of-plane movement in the system after the formation of the 5-5-8 ELD. Further, equilibrium bond lengths and bond angles related to the ELD region predict that like the rest of the system, Si_{ad} and Si_{near} atoms also remain in the sp^2-sp^3 hybridized state (see the Supplemental Material [53] for details). Importantly, the silicene sheet shows rippling, which is well known for 2D structures under finite temperatures [54,55]. Furthermore, as the substrate temperature for deposition of silicene is generally much higher than 300 K, we also perform AIMD at 500 and 1000 K [11,12,25]. It appears that the simulation temperature has little effect on the stepwise formation and the nature of the GB in the reconstruction process.

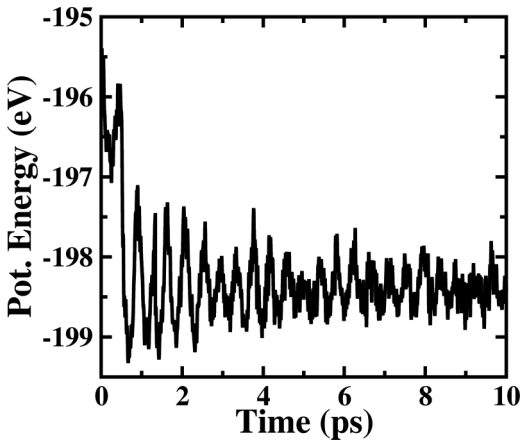

FIG. 3. Total potential energy during AIMD simulations of reconstruction of the ZSi-ZSi GB.

Now, performing a 10-ps-long AIMD simulation for the ASi-ASi structure at 300 K, the GB shows the formation of a stable ELD which contains alternative tetragons and octagons [see Fig. 4(a)]. This kind of ELD has already been found in h-BN sheets after exposing it to electron-beam irradiation at high temperature [33]. Note that Si_{near} atoms involved in tetragonal rings have equilibrium bond angles of $\approx 90^\circ, 135^\circ$, and 135°, which deviate largely from the $\angle \mathrm{Si-Si-Si}$ angle in a pristine sheet, i.e., $\approx 116^\circ$. As these Si_{near} atoms remain in an unfavorable structural situation, the 4-8 ELD remains in a strained condition. However, interestingly, this local strain does not lead to any further structural modifications such as out-of-plane movement of the GB at this temperature. Performing AIMD at 500 and 1000 K, we further confirm that the planar 4-8 ELD is very stable and remains unaltered even at these higher temperatures. Note that Fujimoto *et al.* also predicted a stable 4-8 ring formation in crystalline silicon under tensile stress [56].

For the ZSi-KSi sheet, initial bonds at the GB remain unaltered during AIMD simulation at 300 K [Fig. 4(b)]. However, during equilibration, the GB and its adjacent rings move out of plane significantly (≈ 1 Å). Thus, equilibrated geometry of this sheet shows a huge ripple in the structure [Fig. 4(b)]. Note that here the GB has a four-membered ring containing the ELD (i.e., 4-4-4 ELD) where Si_{near} of a zigzag-edged silicene grain forms four covalent bonds and

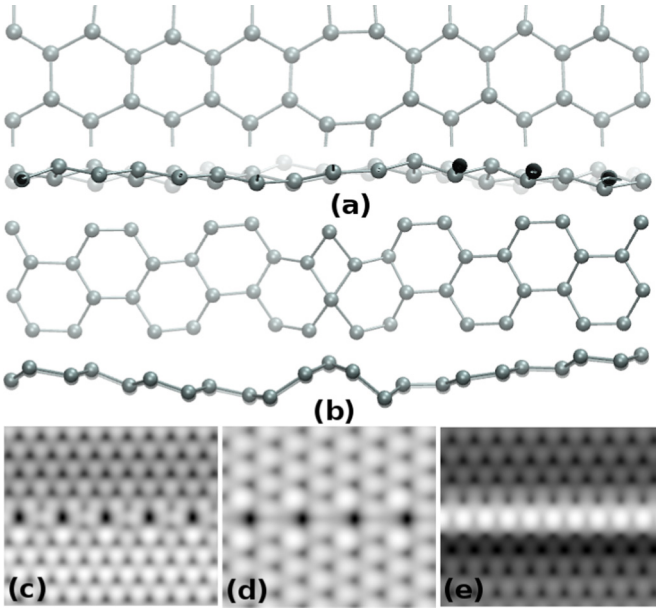

FIG. 4. (Color online) The top and side views of the equilibrated structure (i.e., after 10 ps) of (a) ASi-ASi and (b) ZSi-KSi. Simulated STM images of (c) 5-5-8 ELD, (d) 4-8 ELD, and (e) 4-4-4 ELD are shown. The isosurface is taken at 3.25 Å from the topmost Si atom in all these sheets.

remains in a purely sp^3 hybridized state. Thus, these Si_{near} try to form bond angles $\angle Si-Si-Si \approx 109^\circ$, whereas the planarity of the silicene sheet opposes that by keeping the angles 120° and 60°. As a result, the GB along with other adjacent rings moves out of the plane of the sheet to adjust these two oppositely acting factors. Here one should note that, as Si_{ad} atoms initially do not have bonds with Si_{near} in ZSi-ZSi [Fig. 1(a)], they can move quite freely in the in plane and eventually form a 5-5-8 ELD. However, for ZSi-KSi, all Si_{near} atoms at the GB are covalently bonded during the initial growth process, and any in-plane movement must face high-energy-demanding breakage of covalent bonds. Thus, the GB of ZSi-KSi preferentially moves out of plane and forms high rippling in this 2D sheet. Further, AIMD simulations for all these systems with different ELD-ELD separations show that defect-defect interaction does not have any major impact on the structural reconstructions.

We also theoretically simulate the scanning tunneling microscopy (STM) images of these ELDs containing silicene sheets using the Tersoff-Hamann approximation [57]. STM images are considered to be an efficient tool to identify these defects in various 2D sheets [25,33,58,59]. Figures 4(c)–4(e) show the STM images of these sheets, and the ELD can be identified quite clearly. Note that, as the defect states of these systems stay near the Fermi level (discussed later), ELDs become very prominent in the STM images.

Further, AIMD study at 300 K shows that the reconstructed ZSi-ZSi sheet on the Ag(111) surface becomes structurally distorted after equilibration [Figs. 5(a) and 5(b)]. However, most importantly, the geometry of the 5-5-8 ELD remains almost unaffected in the presence of Ag substrate. The average substrate-silicene distance remains ≈2.3 to 2.8 Å, which is

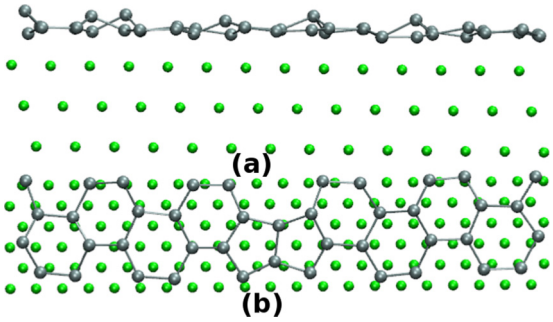

FIG. 5. (Color online) The (a) side and (b) top views of the equilibrated structure (i.e., after 5 ps) of ZSi-ZSi on the surface of Ag(111). Green spheres represent Ag atoms.

slightly higher than in earlier DFT-based calculation due to the finite-temperature effect [11]. Geometries of other ELDs also remain quite unaltered on the Ag(111) surface. As these ELD-containing sheets are quite stable on top of Ag(111), we speculate that field effect transistor of these materials can be fabricated by applying the growth-transfer-fabrication technique as demonstrated by Tao *et al.* [19].

We also investigate the reconstruction process of all these GBs when they appear in the middle of silicene nanoribbons. The GBs of these ribbons transform in identical ways as these evolve in corresponding 2D sheet structures (see the Supplemental Material [53] for details). Moreover, varying the width of two parts of these nanoribbons symmetrically as well as asymmetrically, it is evident that the reconstruction processes are completely independent of the absolute and relative widths of this nanoribbons (see the Supplemental Material [53] for details).

B. Electronic and magnetic properties in 2D sheets

Insertion of line defects in graphene and analogous systems forms localized defect states which result in many exciting phenomena such as spin-polarized electron transport, gate-tunable valley filtration, strain-modulated magnetism, formation of a one-dimensional (1D) channel of free carriers, etc. [36,40,41,60–62]. Thus, it would be interesting to explore the electronic and magnetic properties of different ELDs embedded in silicene and its nanoribbons in search of some emerging technologically important phenomena. To investigate the band structure of these 2D sheets [ZSi-ZSi, for example, in Fig. 6(a)], we consider a rectangular Brillouin zone (BZ) with four high-symmetry k points, as shown in Fig. 6(b). The GB is considered to be periodic along the x axis, i.e., the zigzag (armchair) direction for ZSi-ZSi and ZSi-KSi (ASi-ASi) sheets.

We explore the electronic and magnetic nature of 2D sheets of silicene with the 5-5-8 ELD. Note that, due to the rectangular shape of the BZ, the K point of the hexagonal BZ gets folded at $2\pi/3a$ distance away from the Γ point along the Γ-X line, where a spin-degenerate Dirac point appears in pristine silicene (see the Supplemental Material [53] for details). We denote this point as K''. From the band structure and density of states (DOS) in Figs. 6(c) and 6(d), it becomes evident that, even though all Si atoms are threefold coordinated in the defective sheet, its electronic and magnetic nature largely

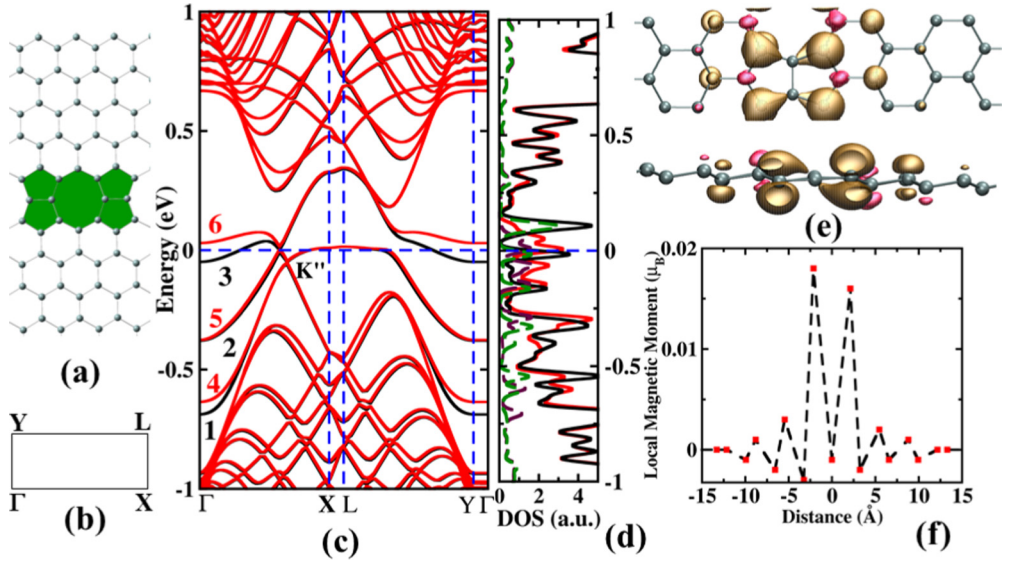

FIG. 6. (Color online) (a) ZSi-ZSi structure with the 5-5-8 ELD (filled green) and (b) the rectangular BZ with high-symmetry k points used here. Spin-polarized (c) band structure and (d) density of state for the 5-5-8-ELD-containing silicene sheet. Black (red) solid lines in (c) and (d) correspond to majority (minority) spin bands and majority (minority) total DOS, respectively. In (d), green (maroon) dashed lines represent the majority (minority) site-projected DOS where the contributions up to the second nearest neighbor of Si_{ad} atoms are summed up. (e) Top and side views of spin densities for ZSi-ZSi, where ochre (red) isosurfaces signify majority (minority) spin. Isosurface value is considered to be 0.001 $e/Å^3$. (f) Local magnetic moment with respect to distance from Si_{ad} dimer atoms. The dimer line of Si_{ad} is considered the origin.

deviates from that of pristine silicene. Near the Fermi level (FL) (i.e., -0.69 to $+0.1$ eV), the spin degeneracy of the energy bands (labeled bands 1–6) gets lifted. The unequal distribution of electrons in these spin-polarized bands results in a finite magnetic moment which will be discussed later on. The bands from both the spin channels, i.e., bands 2, 3, and 5, cross the FL [Fig. 6(c)], demonstrating the prominent spin-polarized metallic nature of the sheet. Moreover, the bands near the FL are dispersive in nature only along the Γ-X and L-Y lines (which are parallel to the direction of the GB). Along the X-L and Y-Γ lines (which are perpendicular to the GB), these bands remain almost nondispersive. In the presence of the 5-5-8 ELD, the hexagonal symmetry of the BZ gets disrupted, and consequently, the exact Dirac point at K'' also disappears. However, a similar kind of band dispersion appears at K'' but -0.05 eV below the FL [see Fig. 6(c)]. Thus, although we find the Dirac-like point at K'', the overall dispersion of these bands get greatly modified due to the insertion of the ELD.

To find the real-space origin of these bands, we analyze their site-projected wave-function characters and band-decomposed charge densities at different high-symmetry k points of the band structure. First of all, as shown in Fig. 7, all the bands near the FL are π bands, i.e., contributed by $3p_z$ orbitals of Si atoms. This is quite natural because unlike point defects, the formation of the 5-5-8 ELD does not introduce any kind of dangling σ bonds in the structure. At the Γ point, all six bands near the FL localize over Si_{ad} and Si_{near} atoms [see Figs. 7(a)–7(c)]. Thus, as all these bands localize at and near the line-defect region, they are considered defect states at the Γ point. However, in the Γ-X direction, i.e., parallel to the ELD, these initially localized states start interacting with other $3p_z$ orbitals of neighboring Si atoms and eventually become delocalized over the whole sheet. This delocalization of charges results in a large dispersion of these bands along that direction of the BZ. Further, as evident from Figs. 7(a)–7(c), along the X-L direction, bands 2 and band 5 remain localized at and near the line defect, whereas the other four bands remain mostly delocalized over the whole structure.

The DOS plot near the FL shows spin-split peaks, indicating breakage of the spin degeneracy in the system [see Fig. 6(d)]. The major peaks of majority and minority spin channels appear below and above the FL, respectively, demonstrating the net spin polarization in the ground state of this sheet. Summing up the contributions of Si_{ad} and Si_{near} atoms to the total DOS, we further find that these peaks are mostly localized around the ELD region and have weak coupling with the rest of the sheet. Thus, the insertion of the 5-5-8 ELD in silicene results in a strongly localized spin-polarized one-dimensional defect channel near the FL of the silicene sheet.

Concentrating on the magnetic properties of the sheet, we find a magnetically ordered ground state with a magnetic moment of $0.2\mu_B$ per unit cell. This magnetic state is lower in energy than the nonmagnetic state by 13 meV/unit cell, which is much larger than in the case of graphene [60,63]. However, the spin-spin interaction in this system is still too weak to maintain magnetic ordering at room temperature, where the spin fluctuation randomizes the direction of spin moments. This interaction can be increased in various ways, such as n-type doping through the gate electrode, applying tensile strain, etc., a subject we will investigate in future studies. The spin density (i.e., $\Delta\rho = \rho_{major} - \rho_{minor}$) of this sheet, as shown in Fig. 6(e), demonstrates a predominant localization of the majority spin at the $3p_z$ orbitals of Si_{near} atoms which ferromagnetically couple along each of as well as across the sides of the Si_{ad} dimer line. One can experimentally detect this local out-of-plane spin ordering by performing magnetic force microscopy (MFM) measurements, which have already been used widely for defective graphene [22]. Now, to obtain

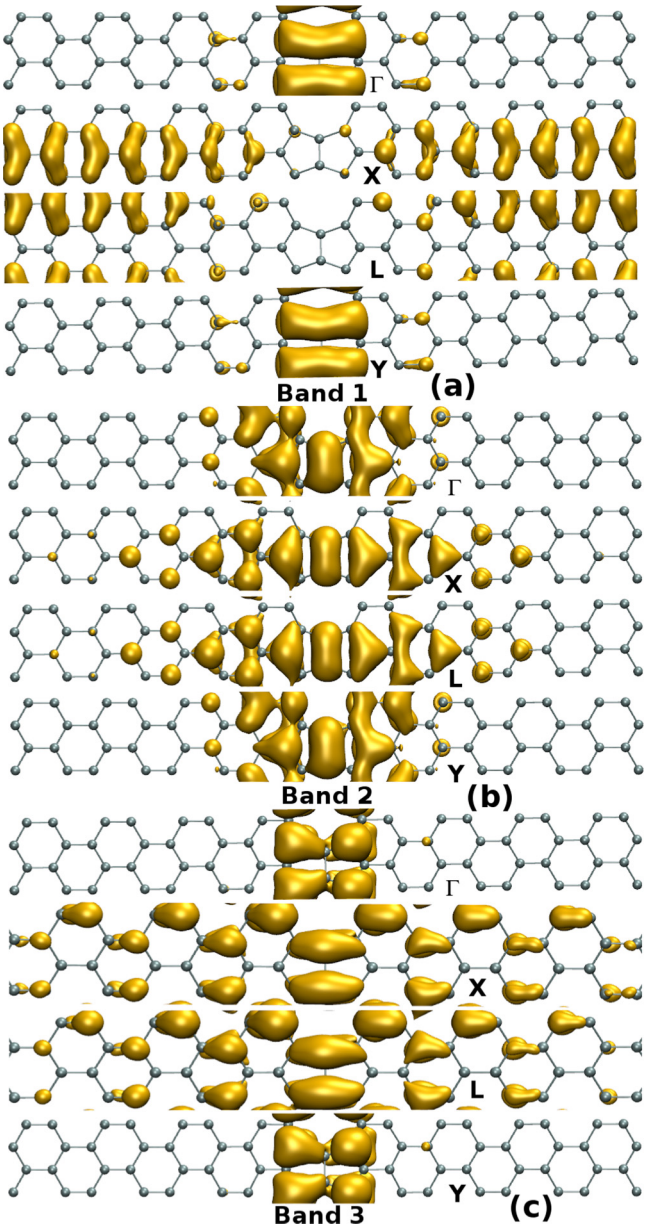

FIG. 7. (Color online) Band-decomposed charge densities of ZSi-ZSi structure with the 5-5-8 ELD at high-symmetry k points for (a) band 1, (b) band 2, and (c) band 3. The isosurface value is considered to be 0.001 $e/\text{Å}^3$ for all charge densities.

a quantitative description, we calculate the magnetic moment distribution around the defect line. We compute the local magnetic moment μ_{local} by defining it as the sum over the magnetic moment of equidistant atoms from the core of the ELD (i.e., Si_{ad} dimer line) divided by the number of equidistant Si atoms. In Fig. 6(f), μ_{local} shows a sharp peak of $0.018\mu_{\text{B}}$ at ± 2.12 Å (i.e., nearest-neighbor distance from the defect core) and then gets reduced sharply in an almost symmetric way on both sides of the ELD with an increase in distance from the defect core.

Note that earlier investigations on graphene containing a 5-5-8 ELD also manifested a prominent ferromagnetic ground state due to spin localization near the ELD line but only under external perturbations such as electron doping, tensile strain, etc. [60,63]. Now the question arises, Why does the 5-5-8 ELD in silicene contain intrinsic spin localization? Here one should consider the difference between graphene and silicene in terms of π bands which involve p_z orbitals of C or Si atoms. As the extent of delocalization of the π bonds in silicene is much less than that of graphene [18], electrons in $3p_z$ orbitals of Si_{near} remain more strongly localized than those in $2p_z$ orbitals of corresponding C atoms. Consequently, this localization of electrons in silicene results in strong electron-electron interaction and a spin split of the π bands near the FL, exhibiting intrinsic magnetic ordering along the 5-5-8 ELD in silicene. Fundamentally, the formation of the 5-5-8 ELD can be visualized as stitching of zigzag edges of two Si grains by Si_{ad} dimers, where either side of the ELD shows pseudoedge-state-like behavior and Si_{near} atoms act as pseudoedge atoms. Further, magnetic moments of individual pseudoedges interact ferromagnetically, giving rise to a spin-polarized metallic ground state. Thus, even though this system does not contain any real edge, electronic and magnetic properties are mostly influenced by these pseudoedge states. Importantly, magnetic properties of these pseudoedge states are more robust than real-edge states as the bulk silicene protects the pseudoedge localized magnetic moments from structural reconstruction or contamination. Therefore, without incorporation of any magnetic adatoms or electron/hole doping, we successfully embed a stable ferromagnetically ordered one-dimensional array of spins just by inserting a 5-5-8 ELD at the silicene sheet. A silicene sheet containing this type of spin channel is very important for future silicon-based spintronics devices.

Concentrating on the 4-8 ELD, the band structure and the DOS plot in Figs. 8(a) and 8(b) evidently demonstrate its metallic nature. Although, like the 5-5-8 ELD, the line defect here does not leave any kind of dangling bond in the structure, the ground state appears to be a nonmagnetic one. In fact, as mentioned earlier, the formation of the 4-8 ELD is a face-to-face (i.e., without any mutual angle) attachment of two armchair edges of silicene sheets. Contrary to the zigzag kind, because armchair edges do not possess any kind of spin localization, the pseudoedge-induced magnetic ordering remains absent in this 4-8 ELD [64]. Note that, in Fig. 8(a), partially occupied band 1 and band 2, which cross the FL, incorporate metallic behavior in the sheet. The site-projected wave-function character and band-decomposed charge densities in Fig. 8(c) identify these bands as π bands, which have major contributions from $3p_z$ orbitals. Figure 8(c) also reveals that both the bands remain delocalized over whole sheet at Γ and Y points and exhibit a highly dispersive nature along the Γ-X and L-Y directions. However, at the X point, these become localized over the ELD and remain nondispersive along X-L. Like the 5-5-8 ELD, dispersive (localized) nature of these bands appears along Γ-X and L-Y (X-L) as the 4-8 ELD is parallel (perpendicular) to these directions. In Fig. 8(b), we also plot the total DOS (black solid line) and projected DOS at 4-8 ELD sites (red dashed line; i.e., the summation of contributions from all Si atoms near the ELD). From Figs. 8(a) and 8(b), it is evident that although the projected DOS of ELD sites contributes little to total DOS near the FL, two peaks at -0.5 and $+0.4$ eV [denoted by asterisks in Fig. 8(b)] appear due to the localization of charge densities at the defect region along the X-L direction.

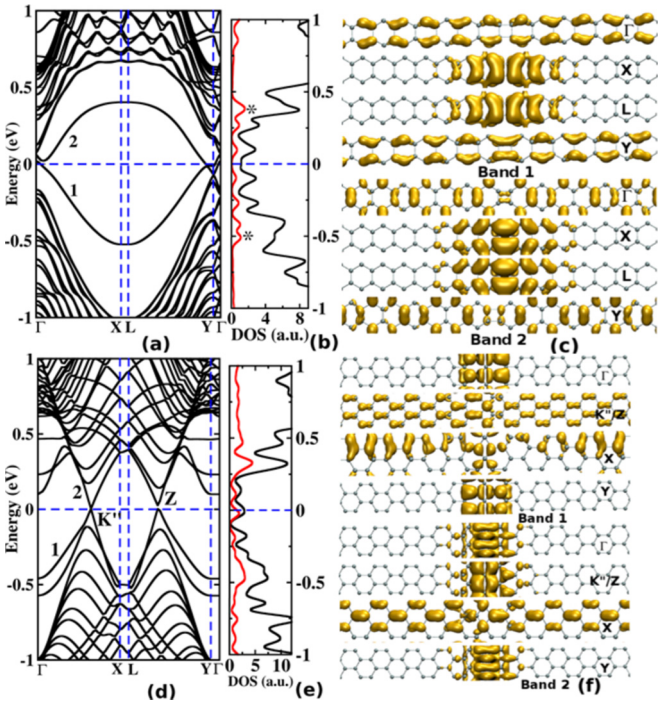

FIG. 8. (Color online) (a), (d) Band structure and (b), (e) total and site-projected DOS for 4-8-ELD- and 4-4-4-ELD-containing silicene sheets, respectively. In the DOS plot, red dashed lines represent the site-projected DOS for which the contribution up to the second nearest neighbors of Si_{ad} atoms are summed up. Band-decomposed charge densities at high-symmetry k points of band 1 and band 2 for (c) ASi-ASi and (f) ZSi-KSi.

Figures 8(d) and 8(e) shows that formation of the 4-4-4 ELD in silicene results in a nonmagnetic metallic state. In the band-structure plot, bands 1 and 2 cross each other (i.e., K'' and Z points) at the FL along the Γ-X and L-Y directions, causing the metallic character of the sheet. Analyzing the site-projected wave-function character and band-decomposed charge densities of these bands at the Γ and Y points, it is evident that two types of orbitals contribute to band 1, (1) $3p_z$ orbitals of Si atoms which are covalently attached to the core of the 4-4-4 ELD and (2) sp^3 hybridized orbitals of Si atoms in the defect core [see Fig. 8(f)]. Band 2 at Γ and Y remains strongly localized at the defect core, where $3s$ and $3p_z$ orbitals of Si atoms hybridize. Importantly, bands 1 and 2, which remain delocalized and localized in nature, respectively, near the K'' and Z points, exhibit band crossing at the FL. In Fig. 8(e), the DOS and the site-projected DOS over the defect region also demonstrate that states near the FL of this metallic sheet are highly localized at the atoms of the 4-4-4 ELD.

C. Electronic and magnetic properties in nanoribbons

As nanoribbons are more relevant than infinite sheets in the field of device applications, we briefly investigate the effects of these line defects in the electronic and magnetic properties of silicene nanoribbons. Due to the sensitivity of these properties to the width of nanoribbons, we also vary the size of the system here. Starting with the 5-5-8 ELD, note that apart from the pseudoedges at the ELD region, now nanoribbons have real edges too. And depending upon the magnetic coupling between two real edges as well as among real and pseudoedges, we can consider different magnetic states such as ferromagnetic coupling among all the edges (FM-1), ferromagnetic coupling between real edges but antiferromagnetic coupling between real and pseudoedges (FM-2), and antiferromagnetic coupling between two real edges (AFM). For a 5-5-ZSi-ZSi-NR (Fig. 9), first, we calculate the relative stability of nonmagnetic (NM), FM-1, FM-2, and AFM states. The magnetically ordered states, i.e., FM-1, FM-2, and AFM states, are more stable than the NM state by 88, 91, and 88 meV/unit cell, respectively. Importantly, the FM-2 state gets stabilized over FM-1 and AFM states by only 3 meV/unit cell. With suitable perturbations such as magnetic field, uniaxial pressure, etc., one can stabilize any of these magnetic states. Thus, we discuss the properties of all the states in detail.

For FM-1 and FM-2 states, the majority-spin band in the valence band (i.e., band 4) at the Γ point has major contributions from $3p_z$ orbitals of Si_{near} atoms, while degenerate band 2 and band 3 originate from zigzag edges (i.e., Si_{edge}; see Fig. 10). As all these bands are localized; they show quite nondispersive, flat-band character near the Γ point [Figs. 9(a) and 9(c)]. However, in the Γ-X direction, like the 2D sheet, these localized bands interact with $3p_z$ orbitals of neighboring Si atoms of the same plane and become quite delocalized and dispersive [see Figs. 9(a), 9(c), and 10]. On the other hand, among minority-spin bands, bands 5 and 6 [localized on Si_{ad} and Si_{near} atoms, respectively (see Fig. 10), at the Γ point], only band 6 becomes delocalized afterwards because it interacts with other Si atoms in the same plane. Further, bands 2 and 3 (bands 7 and 8), which are majority-spin (minority-spin) edge states of the NR, remain almost flat for $0 \leqslant ka \leqslant 0.39\pi$. The degeneracy of edge states near the Γ point appears due to their equivalent geometrical and spin environments. However, this degeneracy gets lifted at $ka > 0.39\pi$, as they interact with other orbitals in different ways. Thus, as is evident from Fig. 10, at the X point bands 2 and 8 become delocalized over the whole nanoribbon, while the other two get localized at the defect region. Now, these spin-polarized bands result in magnetic moments of $1.89\mu_B$ and $0.78\mu_B$/unit cell for FM-1 and FM-2 states, respectively. The spin densities of this nanoribbon also show that the majority spin gets localized on the $3p_z$ orbitals of Si_{edge} for both the FM states [Figs. 9(b) and 9(d)]. However, magnetic coupling between Si_{near} and Si_{edge} atoms shows a ferromagnetic and antiferromagnetic nature for FM-1 and FM-2 states, respectively.

For the AFM state, as shown in Fig. 9(e), bands near the FL disperse quite differently than for the FM states. Unlike the FM states, at the Γ point, edge states of both spin channels become nondegenerate as two edges remain populated with opposite spins facing a nonequivalent spin environment. As a result, one of the majority-spin edge states becomes the valence band, i.e., band 2, whereas the other one, i.e., band 4, remains well above the FL (see the Supplemental Material [53] for band-decomposed charge densities). Importantly, as none of the majority-spin bands cross the FL, an indirect semiconducting gap of 0.11 eV opens up for this spin channel. However, for the minority spin, bands 6 and 7, which originate from both defect and edge orbitals [53], show a highly dispersive nature

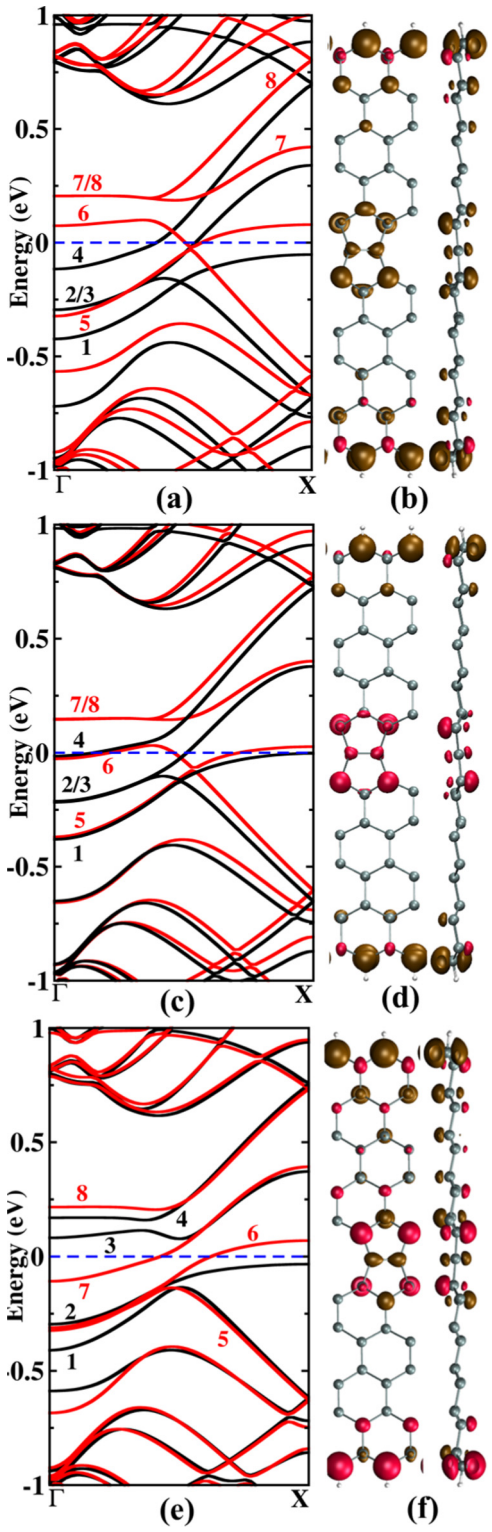

FIG. 9. (Color online) Band structures of 5-5-ZSi-ZSi-NR in (a) FM-1, (c) FM-2, and (e) AFM states. (b), (d), and (f) Top and side views of the spin-density plot for these states, respectively. Ochre and red isosurfaces signify majority and minority spins, respectively. The isosurface value is 0.01 e/Å^3.

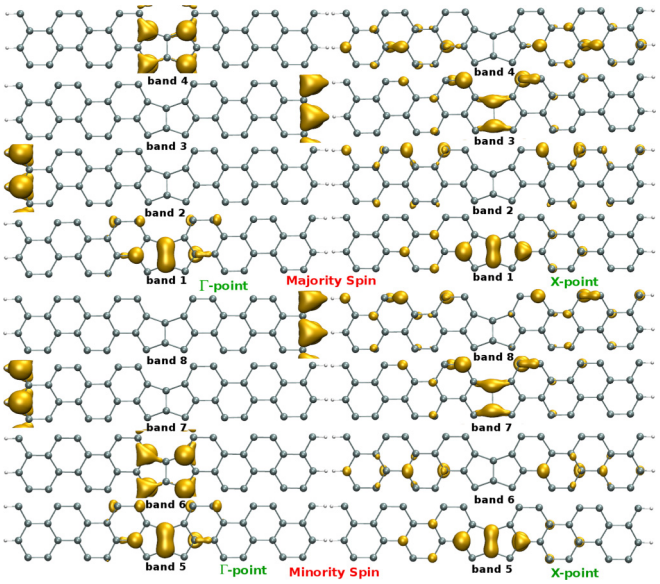

FIG. 10. (Color online) Band-decomposed charge densities at high-symmetry k points, i.e., Γ and X points of 5-5-ZSi-ZSi-NR in the FM-1 and FM-2 states. The isosurface value is 0.0075 $e/\text{Å}^3$.

and cross the FL. As only minority-spin bands populate the FL, this NR shows intrinsic half-metallic character. Note that the half-metallic gap, i.e., the gap between the FL and valence band maxima (VBM) of the majority-spin channel, is 20 meV. Thus, the half-metallic phase needed to be stabilized further by applying some kind of perturbation such as magnetic field or strain. Importantly, as the spin moments of real edges orient oppositely [see Fig. 9(f)], the net magnetic moment becomes $\approx 0\mu_B$/unit cell. Note that, like the 2D silicene sheet with the 5-5-8 ELD, because all these states show an out-of-plane alignment of magnetic moments, the magnetic configuration of the 5-5-ZSi-ZSi-NR can easily be found by performing MFM measurements [22].

Next, we briefly discuss the electronic and magnetic properties for the 10-10-ZSi-ZSi-NR. First, as the spatial separations between two real edges (66.4 Å) and between real edges and pseudoedges (31 Å) are quite large, spin-spin interactions between these edges become negligible. That consequently results in all the magnetic configurations, i.e., FM-1, FM-2, and AFM states, being almost degenerate in energy. Electronically, all these ribbons exhibit a prominent spin-polarized metallic nature (see the Supplemental Material [53] for band and spin-density plots for 10-10-ZSi-ZSi-NRs). Importantly, spin-density distributions in these configurations remain localized to ELDs and edges, similar to narrower ribbons. Note that the half-metallic 5-5-ZSi-ZSi-NR in its AFM state becomes a spin-polarized metal as the ribbon width increases. A similar kind of half-metal to metal transition with the increase in nanoribbon width has also been found in BN-fused polyacene zigzag nanoribbons [65]. Thus, to use this defective SiNR as an intrinsic half-metallic 1D material, nanoribbons must be of smaller width.

SiNRs with the 4-8 ELD and the 4-4-4 ELD appear to be nonmagnetic in their different widths (see the Supplemental Material [53] for band-structure plots). Note that, like pristine systems [64], 4-8-ELD-containing SiNRs appear to be metallic or semiconducting depending upon the number of Si chains

present on two sides of the ELD. However, 4-4-4-ELD-embedded SiNRs are always metallic, irrespective of width.

D. Spin-orbit-coupling effect

To investigate the SOC effect on the electronic properties, we first calculate the band structure of pristine silicene. For the rectangular unit cell of pristine silicene, the orbital degeneracy gets lifted at the K point in the presence of SOC, breaking down the linear dispersion of π bands (formed mainly by $3p_z$ orbitals of Si atoms) near the Fermi level (see the Supplemental Material [53] for band structure). Consequently, a band gap of 1.6 meV appears at the K point. Fundamentally, as π and σ ($3p_x$ and $3p_y$) orbitals of silicene directly overlap due to its buckled geometry, σ-π mixing results in a considerable band gap at the K point. This SOC-induced band structure shows good agreement with other recent studies [10,66].

Now, we concentrate on line-defect-embedded silicene systems where structural symmetry gets destroyed and, consequently, electronic properties deviate a lot from the pristine case due to the appearance of defect bands near the Fermi level. In the following, we discuss the effect of SOC on the defect bands for all the systems. Note that, due to computational limitations, we keep two ELDs eight zigzag/armchair chains apart in 2D sheets during these calculations. For ZSi-ZSi, i.e., the 5-5-8-ELD-containing silicene sheet, SOC modifies the band dispersion near the K'' point [see Fig. 11(a)]. As shown in Fig. 11, near the M and K'' points, two bands [with opposite symmetry when SOC was absent, as seen in the Fig. 6(c)] show an "avoided-crossing" effect, resulting in an energy gap of the order of 2–8 meV, when SOC is introduced. Analyzing the band-decomposed charge densities as shown in Fig. 11(b), quantum tunneling among these SOC-split bands become evident. We find Rashba-type SOC and a $p\pi$-$p\pi$ exchange field as the microscopic reasons behind the observed band lifting. Rashba SOC appears due to the broken structural symmetry of the defect-embedded sheet.

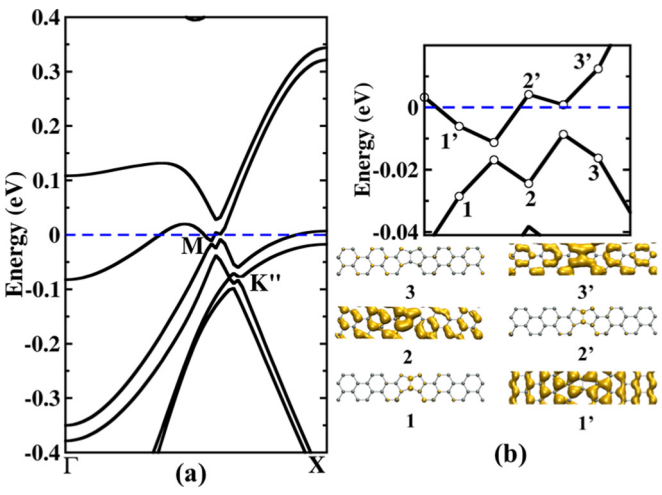

FIG. 11. (Color online) (a) Band structure of ZSi-ZSi considering the spin-orbit-coupling effect. The band dispersion near the Fermi level only through the Γ-X direction is shown here. Band splitting at the M and K'' points is shown. (b) Zoomed-in view of the band near the M point and band-decomposed charge densities of SOC-split bands at particular k points are shown.

However, the effective overlap between spin-polarized defect π states and bulk π states produces the exchange field. Similar kinds of situations arise for transition-metal-doped 2D sheets where both Rashba SOC and the exchange field appear due to the spin-polarized metal atoms [67–69]. Note that, unlike these transition-metal-doped sheets, as the Fermi level stays in the valence band, SOC does not induce band gap for the present system.

For ASi-ASi, defect π bands show an opening of the energy gap near the high-symmetry Y point due to the SOC effect (see the Supplemental Material [53] for band structure). However, the metallic nature and band dispersion through other high-symmetry points remain almost unchanged under the SOC effect for this sheet. In the case of ZSi-KSi, at both the K'' and Z points, where defect π bands cross each other, energy gaps appear due to SOC (see the Supplemental Material [53] for band structure). As in this sheet Si atoms at the defect core remain sp^3 hybridized and the system shows prominent structural distortion, the σ-π mixing become apparently quite strong in nature. Consequently, the band crossings get removed by the incorporation of SOC.

Including SOC for zigzag nanoribbons of silicene with these three different kinds of line defects, we find that the metallic nature of these systems remains unaltered (see the Supplemental Material [53] for band structure).

So for the systems under study, SOC introduces the avoided crossing of bands at certain symmetry points and removes the band crossing and band degeneracy of the energy bands, keeping the overall metallic nature unchanged.

IV. CONCLUSIONS

In conclusion, our room-temperature AIMD studies show that depending upon the nature of GBs in silicene, one can insert different kinds of ELDs, such as 5-5-8, 4-8, 4-4-4, in a controlled way. These ELDs are found to be quite stable at much higher temperatures as well as on the Ag(111) surface. Most importantly, these ELDs can greatly modify the electronic and magnetic properties of a free-standing silicene sheet. Especially, the 5-5-8 ELD shows ferromagnetic ordering of spin moments which are strongly localized at the defect line. Irrespective of the type of ELDs, the Dirac-cone nature of the silicene disappears, and these modified 2D sheets become metallic. Like 2D sheets, SiNRs with different kinds of ELDs are also quite stable at room temperature. Importantly, SiNRs with the 5-5-8 ELD show that differently coupled real edges are almost degenerate in energy. Moreover, stabilizing the antiferromagnetic state for nanoribbons of smaller width, one can achieve a 100% spin-polarized ground state, which is very important for spintronic applications. Last, unlike pristine silicene, the electronic property of all the studied defect-embedded sheets remains unaltered even after considering spin-orbit coupling.

ACKNOWLEDGMENT

S.K.P. acknowledges the Department of Science and Technology, government of India for financial support.

[1] A. K. Geim and K. S. Novoselov, Nat. Mater. **6**, 183 (2007).

[2] K. Novoselov, A. K. Geim, S. Morozov, D. Jiang, M. Katsnelson, I. Grigorieva, S. Dubonos, and A. Firsov, Nature (London) **438**, 197 (2005).

[3] Q. Tang and Z. Zhou, Prog. Mater. Sci. **58**, 1244 (2013).

[4] M. Xu, T. Liang, M. Shi, and H. Chen, Chem. Rev. **113**, 3766 (2013).

[5] A. Kara, H. Enriquez, A. P. Seitsonen, L. L. Y. Voon, S. Vizzini, B. Aufray, and H. Oughaddou, Surf. Sci. Rep. **67**, 1 (2012).

[6] Z. Ni, Q. Liu, K. Tang, J. Zheng, J. Zhou, R. Qin, Z. Gao, D. Yu, and J. Lu, Nano Lett. **12**, 113 (2011).

[7] W.-F. Tsai, C.-Y. Huang, T.-R. Chang, H. Lin, H.-T. Jeng, and A. Bansil, Nat. Commun. **4**, 1500 (2013).

[8] G. G. Guzmán-Verri and L. C. Lew Yan Voon, Phys. Rev. B **76**, 075131 (2007).

[9] S. Cahangirov, M. Topsakal, E. Aktürk, H. Şahin, and S. Ciraci, Phys. Rev. Lett. **102**, 236804 (2009).

[10] C.-C. Liu, W. Feng, and Y. Yao, Phys. Rev. Lett. **107**, 076802 (2011).

[11] P. Vogt, P. De Padova, C. Quaresima, J. Avila, E. Frantzeskakis, M. C. Asensio, A. Resta, B. Ealet, and G. Le Lay, Phys. Rev. Lett. **108**, 155501 (2012).

[12] L. Chen, C.-C. Liu, B. Feng, X. He, P. Cheng, Z. Ding, S. Meng, Y. Yao, and K. Wu, Phys. Rev. Lett. **109**, 056804 (2012).

[13] L. Meng, Y. Wang, L. Zhang, S. Du, R. Wu, L. Li, Y. Zhang, G. Li, H. Zhou, W. A. Hofer, and H.-J. Gao, Nano Lett. **13**, 685 (2013).

[14] A. Fleurence, R. Friedlein, T. Ozaki, H. Kawai, Y. Wang, and Y. Yamada-Takamura, Phys. Rev. Lett. **108**, 245501 (2012).

[15] B. Feng, H. Li, C.-C. Liu, T.-N. Shao, P. Cheng, Y. Yao, S. Meng, L. Chen, and K. Wu, ACS Nano **7**, 9049 (2013).

[16] H. Sahin and F. M. Peeters, Phys. Rev. B **87**, 085423 (2013).

[17] X. Lin and J. Ni, Phys. Rev. B **86**, 075440 (2012).

[18] D. Jose and A. Datta, Acc. Chem. Res. **47**, 593 (2013).

[19] L. Tao, E. Cinquanta, D. Chiappe, C. Grazianetti, M. Fanciulli, M. Dubey, A. Molle, and D. Akinwande, Nat. Nanotechnol. **10**, 227 (2015).

[20] F. Banhart, J. Kotakoski, and A. V. Krasheninnikov, ACS Nano **5**, 26 (2010).

[21] K. T. Chan, J. B. Neaton, and M. L. Cohen, Phys. Rev. B **77**, 235430 (2008).

[22] J. Červenka, M. Katsnelson, and C. Flipse, Nat. Phys. **5**, 840 (2009).

[23] R. Nair, M. Sepioni, I.-L. Tsai, O. Lehtinen, J. Keinonen, A. Krasheninnikov, T. Thomson, A. Geim, and I. Grigorieva, Nat. Phys. **8**, 199 (2012).

[24] F. Hao, D. Fang, and Z. Xu, Appl. Phys. Lett. **99**, 041901 (2011).

[25] D. Chiappe, C. Grazianetti, G. Tallarida, M. Fanciulli, and A. Molle, Adv. Mater. **24**, 5088 (2012).

[26] H. Shu, D. Cao, P. Liang, X. Wang, X. Chen, and W. Lu, Phys. Chem. Chem. Phys. **16**, 304 (2014).

[27] H. Sahin, J. Sivek, S. Li, B. Partoens, and F. M. Peeters, Phys. Rev. B **88**, 045434 (2013).

[28] J. Gao, J. Zhang, H. Liu, Q. Zhang, and J. Zhao, Nanoscale **5**, 9785 (2013).

[29] X. Miao, S. Tongay, and A. F. Hebard, Carbon **50**, 1614 (2012).

[30] L. Wang, X. Zhang, H. L. Chan, F. Yan, and F. Ding, J. Am. Chem. Soc. **135**, 4476 (2013).

[31] P. Y. Huang, C. S. Ruiz-Vargas, A. M. van der Zande, W. S. Whitney, and E. A. Levendorf, Nature (London) **469**, 389 (2011).

[32] J. Lahiri, Y. Lin, P. Bozkurt, I. I. Oleynik, and M. Batzill, Nat. Nanotechnol. **5**, 326 (2010).

[33] O. Cretu, Y.-C. Lin, and K. Suenaga, Nano Lett. **14**, 1064 (2014).

[34] S. Najmaei, Z. Liu, W. Zhou, X. Zou, G. Shi, S. Lei, B. I. Yakobson, J.-C. Idrobo, P. M. Ajayan, and J. Lou, Nat. Mater. **12**, 754 (2013).

[35] O. V. Yazyev and S. G. Louie, Phys. Rev. B **81**, 195420 (2010).

[36] O. V. Yazyev and S. G. Louie, Nat. Mater. **9**, 806 (2010).

[37] Z. Song, V. Artyukhov, J. Wu, B. I. Yakobson, and Z. Xu, ACS Nano **9**, 401 (2015).

[38] Y. Liu, X. Zou, and B. I. Yakobson, ACS Nano **6**, 7053 (2012).

[39] X. Li, X. Wu, X. C. Zeng, and J. Yang, ACS Nano **6**, 4104 (2012).

[40] D. Ghosh, P. Parida, and S. K. Pati, J. Phys. Chem. C **118**, 14670 (2014).

[41] D. Ghosh, P. Parida, and S. K. Pati, J. Mater. Chem. C **2**, 392 (2014).

[42] A. N. Enyashin, M. Bar-Sadan, L. Houben, and G. Seifert, J. Phys. Chem. C **117**, 10842 (2013).

[43] Y. Li, R.-Q. Zhang, Z. Lin, and M. A. Van Hove, Nanoscale **4**, 2580 (2012).

[44] H. Liu, J. Gao, and J. Zhao, J. Phys. Chem. C **117**, 10353 (2013).

[45] A. Podsiadły-Paszkowska and M. Krawiec, Phys. Rev. B **92**, 165411 (2015).

[46] G. Kresse and J. Hafner, Phys. Rev. B **47**, 558 (1993).

[47] J. P. Perdew, K. Burke, and M. Ernzerhof, Phys. Rev. Lett. **77**, 3865 (1996).

[48] P. E. Blöchl, Phys. Rev. B **50**, 17953 (1994).

[49] G. Kresse and D. Joubert, Phys. Rev. B **59**, 1758 (1999).

[50] S. Nosé, J. Chem. Phys. **81**, 511 (1984).

[51] W. G. Hoover, Phys. Rev. A **31**, 1695 (1985).

[52] S. Grimme, J. Comput. Chem **27**, 1787 (2006).

[53] See Supplemental Material at http://link.aps.org/supplemental/10.1103/PhysRevB.92.195136 for figures of 5-5-8-ELD-containing silicene; the reconstruction process in the 5-5-ZSi-ZSiNR, 5-5-ASi-ASiNR, 5-5-ZSi-KSiNR, 10-10-ZSi-ZSiNR, and 16-4-ZSi-ZSiNR; the rectangular unit cell of pure silicene and its band structure; band-decomposed charge densities of the 5-5-ZSi-ZSi-NR; and the band structures of the 5-5-ASi-ASi-NR, 5-5-ZSi-KSi, pristine silicene, ASi-ASi sheet, ZSi-KSi, 5-5-ZSi-ZSi-NR, 5-5-ASi-ASi-NR, and 5-5-ZSi-KSi.

[54] A. Fasolino, J. Los, and M. I. Katsnelson, Nat. Mater. **6**, 858 (2007).

[55] J. Brivio, D. T. Alexander, and A. Kis, Nano Lett. **11**, 5148 (2011).

[56] Y. Fujimoto, T. Koretsune, S. Saito, T. Miyake, and A. Oshiyama, New J. Phys. **10**, 083001 (2008).

[57] J. Tersoff and D. R. Hamann, Phys. Rev. Lett. **50**, 1998 (1983).

[58] D. E. P. Vanpoucke and G. Brocks, Phys. Rev. B **77**, 241308 (2008).

[59] Y. Fujimoto and S. Saito, Phys. Rev. B **84**, 245446 (2011).

[60] L. Kou, C. Tang, W. Guo, and C. Chen, ACS Nano **5**, 1012 (2011).

[61] M. Gibertini and N. Marzari, Nano Lett. **15**, 6229 (2015).

[62] J.-H. Chen, G. Autès, N. Alem, F. Gargiulo, A. Gautam, M. Linck, C. Kisielowski, O. V. Yazyev, S. G. Louie, and A. Zettl, Phys. Rev. B **89**, 121407 (2014).

[63] S. S. Alexandre, A. Lúcio, A. C. Neto, and R. Nunes, Nano Lett. **12**, 5097 (2012).
[64] Y. Ding and J. Ni, Appl. Phys. Lett. **95**, 083115 (2009).
[65] A. K. Manna and S. K. Pati, J. Mater. Chem. C **1**, 3439 (2013).
[66] C.-C. Liu, H. Jiang, and Y. Yao, Phys. Rev. B **84**, 195430 (2011).
[67] Z. Qiao, S. A. Yang, W. Feng, W.-K. Tse, J. Ding, Y. Yao, J. Wang, and Q. Niu, Phys. Rev. B **82**, 161414 (2010).
[68] H. Zhang, C. Lazo, S. Blügel, S. Heinze, and Y. Mokrousov, Phys. Rev. Lett. **108**, 056802 (2012).
[69] X.-L. Zhang, L.-F. Liu, and W.-M. Liu, Sci. Rep. **3**, 2908 (2013).